fire

Article

Structural Performance of Outdoor Mechanical Garages under Combustion Conditions

Yin Zhang [1,2], Zuocai Wang [1,3], Yang Li [1,*], Hongsheng Ma [1] and Zhan Guo [1]

[1] College of Civil Engineering, Hefei University of Technology, Hefei 230009, China; 2020020011@mail.hfut.edu.cn (Y.Z.); wangzuocai@hfut.edu.cn (Z.W.); mahs@mail.hfut.edu.cn (H.M.); 2021170716@mail.hfut.edu.cn (Z.G.)
[2] Anhui Province Infrastructure Safety Inspection and Monitoring Engineering Laboratory, Hefei 230009, China
[3] Anhui Province Road and Bridge Inspection Engineering Research Center, Hefei 230009, China
* Correspondence: liyang.phd@mail.hfut.edu.cn

Abstract: In this paper, the firing process and structural failure behavior of outdoor mechanical car parks are innovatively investigated under diverse conditions, leveraging fire experiments, FDS fire simulation, and finite element simulation. The fire experiments reveal the intricate interplay between flame spread and airflow, highlighting the enhanced risk of fire propagation among adjacent spaces. The temperature profile, mirroring the fire's lifecycle, is delineated into three distinct stages: initial growth, full development, and eventual decay. Notably, full-scale fire simulation in FDS validates the experimental outcomes, underscoring the scalability and reliability of our scaled-down experiments. Furthermore, finite element simulations offer a profound understanding of structural safety in various parking spaces during a fire. Critically, the susceptibility of columns to failure underscores the imperative need for enhanced fire prevention measures in column design, representing a significant advancement in fire protection engineering.

Keywords: failure behavior; firing process; temperature variation; structural safety; flame spread

check for updates

Citation: Zhang, Y.; Wang, Z.; Li, Y.; Ma, H.; Guo, Z. Structural Performance of Outdoor Mechanical Garages under Combustion Conditions. *Fire* **2024**, *7*, 116. https://doi.org/10.3390/fire7040116

Academic Editors: Manhou Li and Weiguang An

Received: 4 February 2024
Revised: 27 March 2024
Accepted: 1 April 2024
Published: 2 April 2024

Copyright: © 2024 by the authors. Licensee MDPI, Basel, Switzerland. This article is an open access article distributed under the terms and conditions of the Creative Commons Attribution (CC BY) license (https://creativecommons.org/licenses/by/4.0/).

1. Introduction

With the acceleration of urbanization and the increase in the number of automobiles, outdoor mechanical car parks have gradually become one of the common infrastructures in urban public places and residential communities, providing convenience for car parking [1]. However, the risk of fire in outdoor mechanical car parks is also increased during usage. Fires not only cause casualties and property damage, but can also significantly impact a city's overall safety. Therefore, conducting in-depth research on fire safety issues in outdoor mechanical car parks and improving their safety prevention technology are deemed significant.

Fires in mechanical car parks generally occur due to the spontaneous combustion of parked cars. The generation of a large amount of high-temperature gas and a source of fire through spontaneous combustion and burning severely affects the steel structural components of the mechanical parking spaces and the surrounding environment. The steel structural materials are heated by the spread of high-temperature gas and fire sources, leading to material expansion, deformation, instability, and detrimental effects on the overall stability of the parking spaces. Additionally, in high-temperature environments, thermal radiation and smoke pose risks of harm to vehicles and personnel. Therefore, systematic research into and analysis of the high-temperature effects of spontaneous combustion and the burning of cars on the steel structures of mechanical parking spaces hold both theoretical and practical significance. Currently, research has been conducted by the academic community on the high-temperature effects of spontaneous combustion and the burning of cars on the steel structures of mechanical parking spaces. Wang et al. [2] studied the influence of the opening size of a passenger car compartment on fire behavior using a scaled-down car model and six fire experiments. Zhu et al. [3] investigated the combustion behavior and fire spread characteristics of moving vehicles. The progress of the fire was recorded through cameras installed at different angles, and the temperature was measured using thermal imaging and thermocouples. Terziev et al. [4] proposed a comprehensive experimental method to study the impact of a vehicle fire on adjacent vehicles. Temperature measurements were conducted using 16 thermocouples and thermal imaging cameras, with a focus on studying the heat flux released by burning vehicles to adjacent vehicles at specific distances between vehicles. Okamoto et al. [5] conducted two full-scale vehicle fire experiments using a small multifunctional car and measured the surrounding heat flux. The methods were proposed to simulate and calculate the flame shape, temperature, and lateral heat flux in a combustion vehicle. Brzezinska et al. [6] reviewed 44 full-scale car fire experiments and passenger car fire statistics from Poland and the UK from the past 8 years. Based on the collected data and average experiment results, the relevant heat release rate (HRR) was summarized as a reference value, providing assistance for local governments and stakeholders in determining the optimal fire safety design standards for parking lots. Truchot et al. [7] conducted full-scale experiments on a van fire and obtained a peak heat release rate of up to 3.38 MW when gasoline leaked. For the first time, the average radiation scores during the intense combustion phase of the engine compartment and passenger compartment were determined to be 0.469 and 0.589, respectively. From this, it can be determined that the thermal radiation and fire safety distances of personnel and adjacent vehicles in the spatial position on the side of the vehicle are approximately 7.3 m and 2.1 m, respectively. Dorsz et al. [8] analyzed the fire hazards of electric vehicles operating in enclosed spaces, with a focus on personal and property safety. The characteristics, heat release rate, total heat release, and factors affecting the development of electric vehicle fires were investigated. The impact of these parameters on the safety of closed structures was evaluated using CFD simulation. Li et al. [9] conducted full-scale fire experiments on two four-door sedans placed side by side to investigate the diffusion behavior of flames and smoke temperature. It was observed that the flame propagated faster through the roof than the bottom of the carriage, while the fire slowly spread from the engine compartment to the carriage. The peak temperature inside the vehicle reached 900 °C.

The fire safety performance of outdoor mechanical car garage steel structures is significantly influenced by the thermal responses and effects caused by fires. Factors such as high temperature, smoke, and splashes in fires not only alter the material physical properties of the structure [10–12], but also alter the stress state of the structure, leading to structural failure [13–16]. In various studies, researchers at home and abroad used the method of numerical simulation to analyze the temperature distribution and deformation characteristics of the steel structures of mechanical parking spaces under fire conditions in high-temperature environments, which provides an important reference basis for evaluating the fire safety performance of steel structures [15–18]. In addition, through actual fire testing and laboratory simulation experiments, the thermal response and instability characteristics of steel structural components during fire propagation were thoroughly studied [19,20]. However, several unresolved issues persist in practical applications, including insufficient experimental data on outdoor automobile mechanical garage fires and the influence of different physical parameters on fire development.

The application of FDS in automotive fire simulation is extensive [14], and numerous studies have already employed the FDS method. Selamet et al. [21] estimate fire spread in automated multi-story parking garages, revealing that steel pallets can reach extreme temperatures, causing structural failure. Koromila et al. [22] established fire safety assessment procedures for Ro-Ro ship cargo spaces, leveraging vehicle fire data to derive heat release rates and simulating fire propagation on ship decks using FDS. Gavryliuk et al. [23] simulated the characteristics of electric vehicle fires using FDS, taking Tesla Model S as an example. It was found that, in order to ensure safety, the minimum fire protection distance between electric vehicles and various types of building walls should be at least 3 m, provided that the free fire development time is 600 s. Di Matteo et al. [24] employed Fire

Safety Engineering methods like Pyrosim and FDS to simulate and analyze fire behavior in enclosed spaces. This study developed a simulation model to analyze fire behavior and weaknesses in suppression systems, emphasizing the need for continued research and development to enhance safety. Ma et al. [25] employed numerical simulation methods to thoroughly investigate the evolution of bridge deck fires in a fully open environment and construct a simplified fire model that comprehensively considers the effects of wind. Through simulation and verification, it was discovered that wind effects have a significant impact on the combustion process of fires.

In pertinent research, it has been found that finite element analysis holds a prominent position in simulating heat transfer mechanisms, structural responses, and the propagation of fire during the occurrence of mechanical garage fires. Xia et al. [15] analyzed the thermal exposure of steel framing members in open parking fires using a CFD-FEM coupled model, considering the impact of galvanization on steel temperature changes. Ayva et al. [26] used fire simulation and finite element analysis to identify the thermal conditions necessary for a vehicle fire to extend to adjacent and overhead parking decks. Additionally, they analyzed the collapse mechanism of the parking deck under such fire conditions. Kumar and Kodur [27] proposed a rational method for evaluating the fire resistance of double-T prestressed concrete slabs in parking structures. This method employs a finite element analysis numerical model to simulate the fire resistance of double-T slabs under various fire and load scenarios. Meng et al. [28] established a finite element model through the finite element method to simulate the performance of an eight-bay parking frame under two different fire scenarios. Evidently, the finite element method has gradually emerged as an indispensable and crucial tool for the thorough investigation of the high-temperature performance of garages.

To investigate the development patterns and thermal effects of structural fires in outdoor mechanical car parks and further enhance fire safety prevention technology, experimental and simulated studies will be carried out in this paper. By controlling fire conditions and monitoring parameters, the development law of mechanical garage fires and the response laws to environmental factors are explored. Additionally, computer simulation techniques [29,30] are utilized to establish a thermal response model for the steel structures of outdoor mechanical car garages under fire conditions. The temperature distribution and stress response laws of the steel structures of mechanical garages under fire conditions are analyzed to provide a theoretical basis for improving the fire safety performance of mechanical garages.

2. Small-Scale Fire Design of Experiments

2.1. Small-Scale Fire Design of Experiments

2.1.1. Experimental Model Design

Outdoor mechanical car garages are mostly steel structures, as shown in Figure 1a. To study the fire effect of cars in outdoor mechanical car garages, a locally scaled model of a three-dimensional parking garage is designed and established in this paper. According to the JGJ 100-2015 Code for Design of Parking Garage Building [31] and the GB50067-97 Code for Fire Protection Design of Garage, Motor RepairShop and Parking Area [32], the size of the parking space was set at $5.4 \times 2.25 \times 1.6$ m.

In accordance with the Froude similarity criterion, the scaled-down fire experiment was conducted with strict adherence to prescribed methods and criteria to ensure precision and reliability. A scale ratio of 1:5 was used to maintain the proportionality of the inertial and gravitational forces between the prototype fire scenario and the scaled model. Geometric configurations and fire properties resembling the prototype were utilized to mimic real-world fire dynamics. The Froude number, representing the ratio of inertial to gravitational forces, was calculated and maintained constantly to ensure analogous fire behaviors in the scaled model, as shown in Equation (1). Rigorous control measures and advanced measurement techniques were implemented to enhance the accuracy and reproducibility of the experiment. By adhering to these rigorous methods, we aimed to achieve accurate and reliable experimental results that offer valuable insights into the fire dynamics of the prototype scenario.

$$Fr = \frac{U_0}{\sqrt{g_0 L}} \tag{1}$$

where U_0 represents the flow velocity; g_0 represents the acceleration of gravity; and L represents the characteristic.

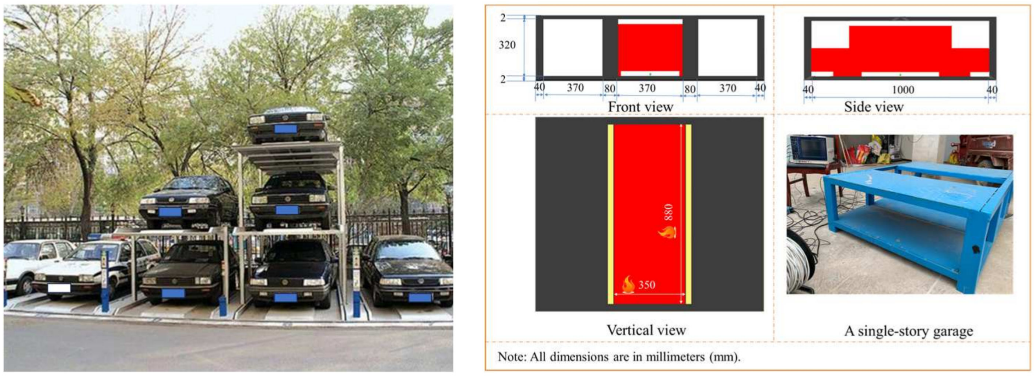

(**a**) (**b**)

Figure 1. Experimental design of outdoor mechanical car parking garage: (**a**) an actual mechanical parking space and (**b**) scale design of experiments.

The mechanical garage model was established at a scale of 1:5. The model structure and dimensions in millimeters are shown in Figure 1b. The local model includes the leftmost parking spaces of P1 and P4, the rightmost parking spaces of P3 and P5, and the middle lift-shaft parking space of P2. The top of the lifting well parking space P2 is hollowed out without a board wall. The other parts of the frame are made of a Q235 steel structure. To simulate a car fire, a fuel pool was set up with a 1:5 reduction in car size, with a projected size of 4.4 × 1.75 m scaled to 880 × 350 mm. As a fundamental research method, the pool fire experiment has extensive applications in fire science, facilitating the understanding of fundamental physical processes like flame propagation and temperature distribution. To investigate the basic laws governing fire spread and mechanical structure response, a pool fire was employed in this study to simulate the initial stage of a vehicle fire. Despite differences in heat release rate profiles [33–35], the pool fire retains a certain degree of representativeness during its early stages.

2.1.2. Case Condition Design

Currently, automotive fires can be categorized into two major types based on their power sources: those induced by the combustion of fuel [36], and those triggered by flammable gases resulting from thermal runaway in new energy vehicle batteries [37]. It is noteworthy that there are significant differences in the induction mechanisms and fire characteristics between gasoline-dominated fuel fires and electric vehicle fires caused by flammable gases. As a representative of the commonly used fuel in automobiles, gasoline occupies a dominant position in the combustion characteristics of fuel fires. The simulation experiments with gasoline can better replicate actual fuel fire scenarios. Furthermore, by controlling experimental conditions, the boundaries are effectively established for the experimental environment, ensuring the accuracy and reliability of the experimental results. This controllable boundary allows for a deep investigation into the occurrence, development, and spread of fuel fires, providing a scientific basis for preventing and responding to actual fires. Additionally, gasoline is easily accessible, and simulating automobile fires using gasoline also exhibits high experimental reproducibility. However, it is worth mentioning that the simulation of new energy vehicle battery fires [35] is closely related to gas diffusion and combustion characteristics, which significantly differs from traditional fuel pool fire simulations. Therefore, the study of fuel fires is primarily focused on in this paper.

The parking spaces of the model garage are numbered P1, P2, P3, P4, and P5, as shown in Figure 2. A camera system, combustion experimental area, and temperature measurement system are included in the experimental platform. The Sony HXR-NX100 camera, manufactured by Sony Corporation in Tokyo, Japan, is precisely placed 15 m away from the target flame. According to the brightness of the experimental environment, the focal length and aperture are adjusted to appropriate parameters to ensure clear recording of the entire combustion process. After calibration, thermocouples are installed at the center of each parking space to accurately monitor temperature changes. The fuel pools are made of fire-resistant materials and filled with a fixed amount of gasoline. A unified fuel volume of 5 L is assigned to the parking spaces. Ignition is achieved using a stable electric spark igniter. The experiments are conducted in an open outdoor environment in a selected time period with minimal wind and a suitable temperature. Windshield measures are also taken to reduce interference. The experimental site is equipped with emergency equipment, including dry powder fire extinguishers, carbon dioxide fire extinguishers, and water mist cannons. The experimental personnel underwent safety training to ensure the safety and controllability of the experimental process. These carefully designed details ensure the accuracy and reliability of the experiments.

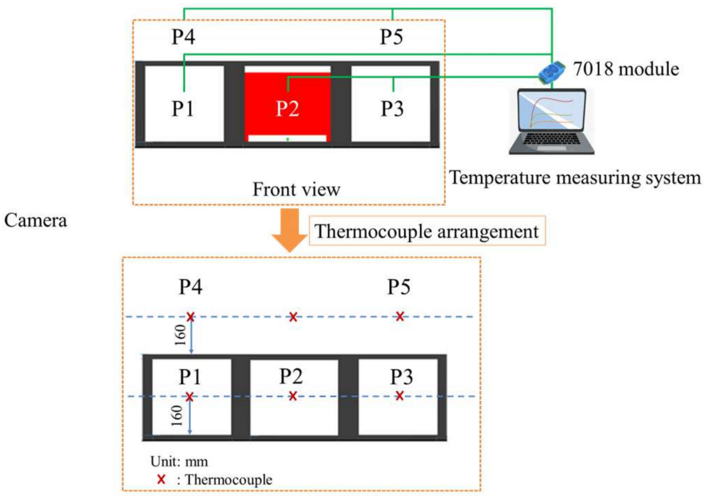

Figure 2. Layout of measurement points.

To study the impact of flame propagation on the high-temperature characteristics of the garage during car combustion, 3 case conditions are set up for small-scale experiments, as shown in Table 1. Given the open nature of mechanical parking spaces, the design of these experiments particularly considers the horizontal and vertical spread of fire. To effectively simulate this, a scaled-down model of a double-deck mechanical garage with 5 parking spaces is used, allowing for ignition at different locations. In Case 1, the fuel pool is placed in parking spaces P1, P2, and P3, and parking space P2 is ignited. In Case 2, the fuel pool is placed in parking spaces P1, P3, and P5, and parking space P3 is ignited. In Case 3, the fuel pool is placed in parking spaces P3, P4, and P5, and parking space P5 is ignited. The thermocouples for parking spaces P1, P2, P3, P4, and P5 are located 0.16 m away from the bottom plate at the same level. The ignition fuel is selected as 92# gasoline, and the camera is located directly in front to record the firing process. The experimental platform is located in an open outdoor environment. To avoid interference from multiple factors, a calm or breezy state should be chosen for the combustion experiments. The ambient temperature during the experiment was 18 °C, with a northern gust of minimal wind speed.

Table 1. Design of case conditions.

Case	Fuel Pool Location	Ignition Position	Illustration	Individual Fuel Pool Size (mm × mm)
1	P1, P2, P3	P2		
2	P1, P3, P5	P3	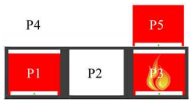	880 × 350
3	P3, P4, P5	P5	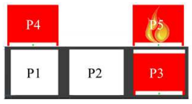	

2.2. Analysis of Experiment Results

2.2.1. Experimental Flame Behavior

In the experiment, 3 fire stages are experienced sequentially, namely the initial growth stage, the fully developed stage, and the decay stage [38]. In relatively enclosed building fires, there is also a flashover stage. Due to the sufficient oxygen supply in the outdoor open environment of the mechanical garage, the flashover stage is missing. The gasoline fuel in the experiment was directly ignited, resulting in no smoldering stage. However, in actual car fires, there may be a smoldering stage. From the fire in the independent parking space shown in Figure 3, it can be observed that there are significantly different fire intensities in different fire stages.

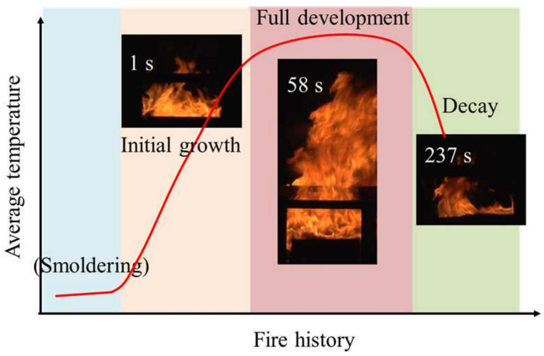

Figure 3. Process of a fire in an independent parking space.

In the initial stage of fire development, oxygen is fully supplied and the fire intensity gradually increases. Due to the opening of the top of parking spaces P2, P4, and P5, a large amount of thick smoke can escape with the movement of the flame plume zone. Conversely, P1 and P3 have obstacle walls at the top, creating a confined space where smoke accumulates, escapes, and generates strong convection, thereby enhancing the fire's intensity.

After the fire enters the full combustion stage, the combustion intensity continues increasing. Subsequently, the heat release rate gradually reaches a certain maximum value and remains stable. This severe heat damages the mechanical structure, allowing high-temperature fire and smoke to spread, intensifying and expanding the blaze. In the worst scenario, the entire mechanical garage catches fire, possibly collapsing.

In the final stage of the fire, the combustible materials gradually burn out, and the fire enters a weakened period. The temperature of the parking space also quickly decreases. The combustion rate decreases, gradually extinguishing the flame. However, residual heat and smoke persist, posing continued risks.

The fire progression of Case 1 is shown in Figure 4a. A fuel volume of 5 L is assigned to parking spaces P1 and P2, while a fuel volume of 5 L is in P3. In the initial moment, the fire originated in parking space P2, indicating the initial growth stage of the fire. Within the following 2 s, the flame started to spread toward parking space P3. At 34 s, the flame spread to parking space P1. Because P3 was located downwind while P1 was upwind, parking space P3 was ignited before parking space P1. Although the wind speed was very weak, the P3 parking space was quickly ignited with the pulsation of the flame along with the airflow. The natural winds were not continuous. When the gust halted, the flames in parking space P2 quickly returned to their original position. Since there was no obstruction directly above parking space P2, the flame burned vertically from the opening, forming a plume. However, the width of the flame was much greater than the width of the orifice. Therefore, when there is no wind and stable combustion, the steel wall on top of the P1 parking space will be hit by the flame of the P2 parking space, causing a wall collision flame. Furthermore, the flame was sucked towards the P1 parking space, leading to the ignition of the P1 parking space. The fully developed stage of fire was reached at 46 s and continued for a total duration of 252 s until complete extinguishment. Due to the generation of a large amount of smoke, the bright yellow color of the flame transitioned to a dark red color.

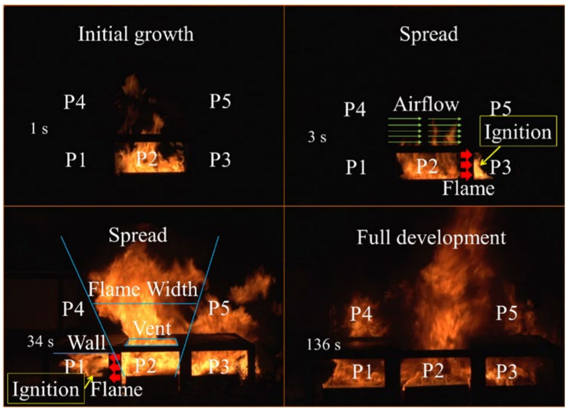

(**a**)

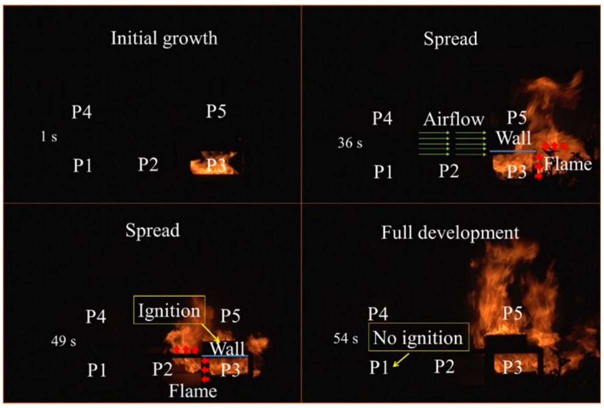

(**b**)

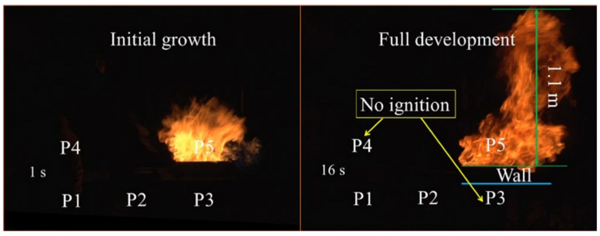

(**c**)

Figure 4. Fire occurrence process under different case conditions: (**a**) Case 1, (**b**) Case 2, and (**c**) Case 3.

Figure 4b depicts the fire progression of Case 2. The fuel volume of parking spaces P1, P3, and P5 is 5 L. The fire originated in parking space P3 at the initial moment, exhibiting intense movement influenced by a gentle airflow. Due to the absence of any obstructions, the flames collided with the wall and fled towards the surrounding area along the top wall. The spreading flame was uplifted with buoyancy. Therefore, the adjacent upper P5 parking space was ignited at 49 s by the diffusion flame of P3. Subsequently, parking spaces P3 and P5 entered the fully developed stage together and continued to burn for 233 s before extinguishment. Parking space P1 remained unignited throughout the entire duration. This indicates that adjacent parking spaces are more prone to fire spread, and spaced parking spaces can effectively block fire spread.

Figure 4c presents the fire progression of Case 3. In the initial moment, parking space P5 ignited with a bright yellow flame. After 16 s, the fire in parking space P5 reached the fully developed stage, generating a large amount of smoke and a dark red flame. Due to the absence of obstacles in the upper part of parking space P5, the maximum flame height during the completely open combustion period was about 1.1 m. However, parking space P4 remained unignited throughout the entire duration, confirming the conclusion that spacing between parking spaces contributes to fire prevention. Additionally, parking space P3 was also not burned throughout the fire event. This can be attributed to the strong influence of buoyancy on the flame of the liquid fuel, primarily affecting the upper-level structures, while the lower-level structures experienced minimal impact even in adjacency. Therefore, this indicates that fires rarely spread from top to bottom.

2.2.2. Temperature Distribution

The temperature measurement data are, respectively, plotted in Figure 5. It can be observed that the temperature curves closely follow the flame behavior and exhibit 3 stages of fire progression: ignition, full fire development, and fire decay. Figure 5a displays the temperature curves of parking spaces P1 to P5 for Case 1. The temperature of parking space P2 sharply increases after ignition. Because the ignition time of the P3 parking space is only 3 s behind that of the P2 parking space, the heating trend of the P3 parking space is slightly delayed by the temperature curve of the P2 parking space. After 34 s, the temperature of parking space P1 starts to increase rapidly. Since parking spaces P4 and P5 are not burned, the temperature increase mainly results from thermal radiation and conduction from other parking spaces. The temperature of parking space P5 is mainly influenced by the flames in P2 and P3, while the temperature of parking space P4 is primarily affected by the flames in P2 and P1. The delayed ignition and thermal convection of parking space P1 are the main reasons for the delayed and lower heating curve of parking space P4 compared to parking space P5. Figure 5b presents the temperature curves of parking spaces P1 to P5 for Case 2. The time interval between ignition in spaces P3 and P5 is approximately 49 s, which is consistent with the observed flame behaviors. As P2 is adjacent to a burning flame, its temperature rises slowly and reaches its peak at 342 s. Since P1 and P3 are farther from the burning flame, their temperature increase is not significant, with the highest temperature recorded being only 57 °C. Figure 5c shows the temperature curves of parking spaces P1 to P5 for Case 3. Parking space P5 is the ignition source, and its temperature rise behavior is consistent with the ignition locations observed in other case conditions. Due to the presence of a vent at the top of P2, there are no obstructions hindering temperature rise, resulting in a gradual increase until the peak is reached at 274 s. As parking space P4 is located far from P5, the temperature rise is not prominent. Although the P3 parking space is adjacent to the open flame of the P5 parking space, both thermal radiation and conduction are obstructed by the top wall. In addition, the temperature is also weakened by thermal convection, making it difficult for the P3 parking space to experience a temperature rise. The characteristics of parking spaces P4 and P3 are reflected in parking spaces P1, resulting in no significant temperature changes.

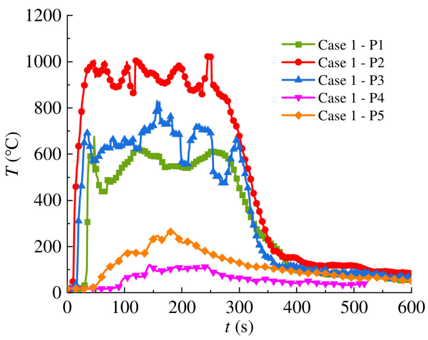

(**a**)

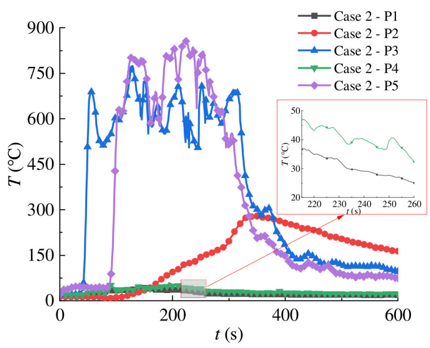

(**b**)

Figure 5. *Cont*.

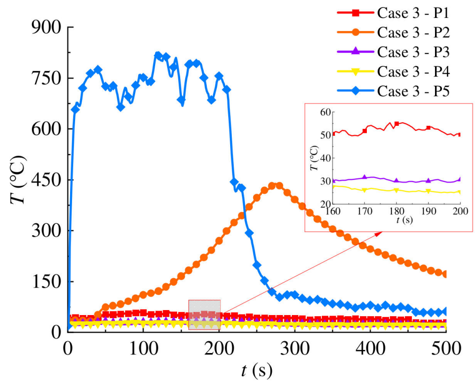

(**c**)

Figure 5. Temperature profiles under different case conditions: (**a**) Case 1, (**b**) Case 2, and (**c**) Case 3.

3. Fire Simulation in FDS

3.1. FDS Modeling

Fire Dynamics Simulator (FDS) is a computational fluid dynamics tool that simulates fire from ignition to flame propagation, providing insights into fire dynamics. The simulation calculation is configured with a high-performance computing system, equipped with 32.0 GB of RAM and a 12th Gen Intel Core i7-12700 processor sourced from Intel Corporation, headquartered in Santa Clara, United States. A full-scale model in FDS was established, as shown in Figure 6a,b. Each parking space measures 5.4 × 2.25 × 1.6 m, providing sufficient space for a realistically modeled car with dimensions of 4.4 × 1.75 × 1.45 m. To ensure the accurate representation of fire behavior, the thermocouple position, as shown in Figure 6c, is at the center of the cross-section of the parking space, replicating the experimental setup. The computational domain, measuring 8 × 7 × 5 m, encompasses the entire fire scenario. A grid size of 0.2 m is chosen, resulting in 35,000 grid cells.

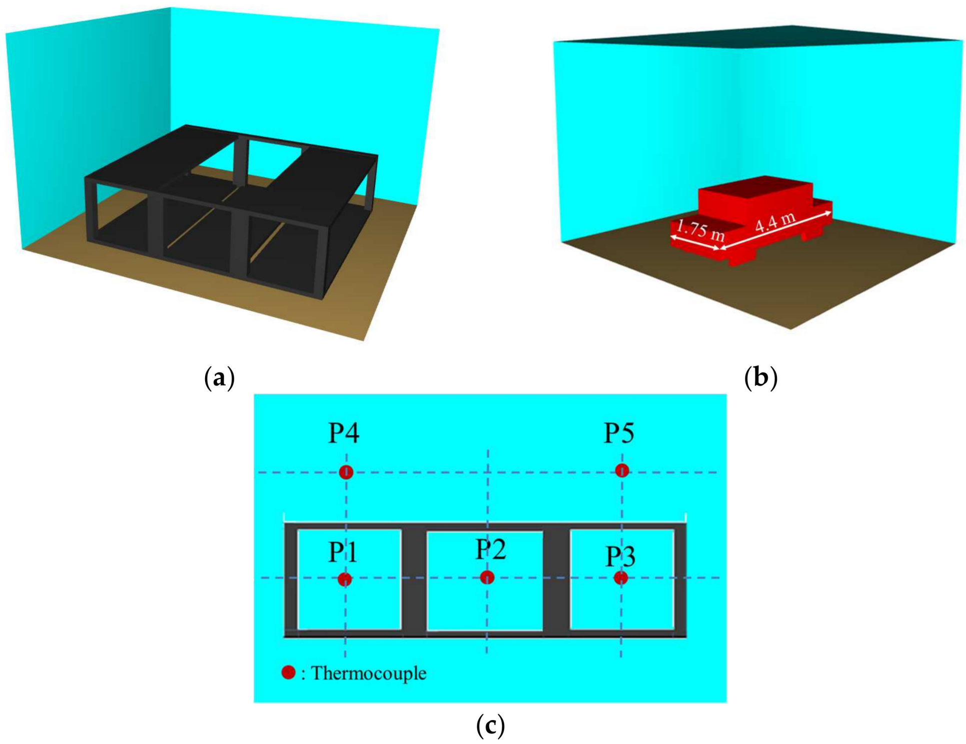

Figure 6. Local framework model of the horizontal mechanical garage: (**a**) mechanical parking space modeling, (**b**) car modeling, and (**c**) thermocouple positions.

To accurately simulate the fuel properties of gasoline, its flash point is set at 427 °C under normal atmospheric pressure. Moreover, the calorific value of gasoline, approximately 44.15 MJ/kg [39], is taken into account in the simulation. This value determines the amount of heat released per unit mass of gasoline burned, which is crucial in calculating HRR, as shown in Equation (2). It is generally considered that the maximum HRR for car fires is 3 MW [40].

$$Q = A \times m'' \times \chi \times \Delta H_c \tag{2}$$

where Q represents HRR in Figure 7 [41], which belongs to the ultrafast fire in this paper; A represents the projected combustion area; m'' represents the mass loss rate per unit area of the large fuel pool (>5 m^2), taken as 0.055 $kg \cdot m^{-2} \cdot s^{-1}$; χ represents the combustion efficiency, taken as 70% for gasoline; and ΔH_c represents the heat of combustion for gasoline.

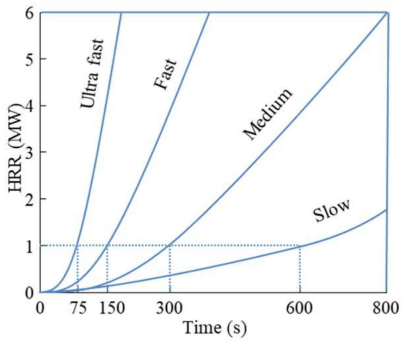

Figure 7. t^2 fires.

The use of the t^2 fire in the FDS simulation is widely practiced in fire science research, especially when simulating specific scenarios like car fires [35]. Non-steady-state fires can be represented as t^2 fires, and during the initial growth stage of a fire, the HRR approximately follows a t^2 relationship with time [41,42]. Therefore, the fire growth curve is expressed by Equation (3). By the calculations, the time to reach the maximum HRR of 3 MW for t^2 fires in car combustion is 46 s.

$$Q = \alpha t^2 \tag{3}$$

where α represents the fire growth coefficient with a corresponding value of 0.1878; t represents the duration after the fire occurred; and t_0 represents the time when the fire occurred.

3.2. Results Analysis of FDS

3.2.1. Flame Behavior in FDS

Figure 8 illustrates the simulation process of the fire initiation, spread, full development, and decay stages. The full-scale simulation results are found to be in good agreement with the reduced-scale experimental fire progression. Figure 8a shows that the flame in Case 1 is slim for the first 10 s, gradually developing as the fire progresses. At 35 s, the fire spread from parking space P2 to P3. At 67 s, the P1 parking space was ignited by a spreading flame in the P2 parking space. Then, the fires in P1, P2, and P3 merged, entering the full development stage of the fire. Finally, the fire was weakened and extinguished at 300 s. Figure 8b demonstrates that some smoke in Case 2 was generated at 20 s. At 67 s, the fire spread from P3 to P5. By 107 s, the fires in P3 and P5 had merged and reached the full development stage. After a stable period in the full development stage, the flame is shown to weaken and extinguish at 360 s. According to Figure 8c, the flame in Case 3 becomes evident and enters the initial growth stage at 10 s. Due to only one parking space (P5) being burned, it quickly reaches the full development stage at 38 s. Finally, the flame is weakened and extinguished near the 264 s mark.

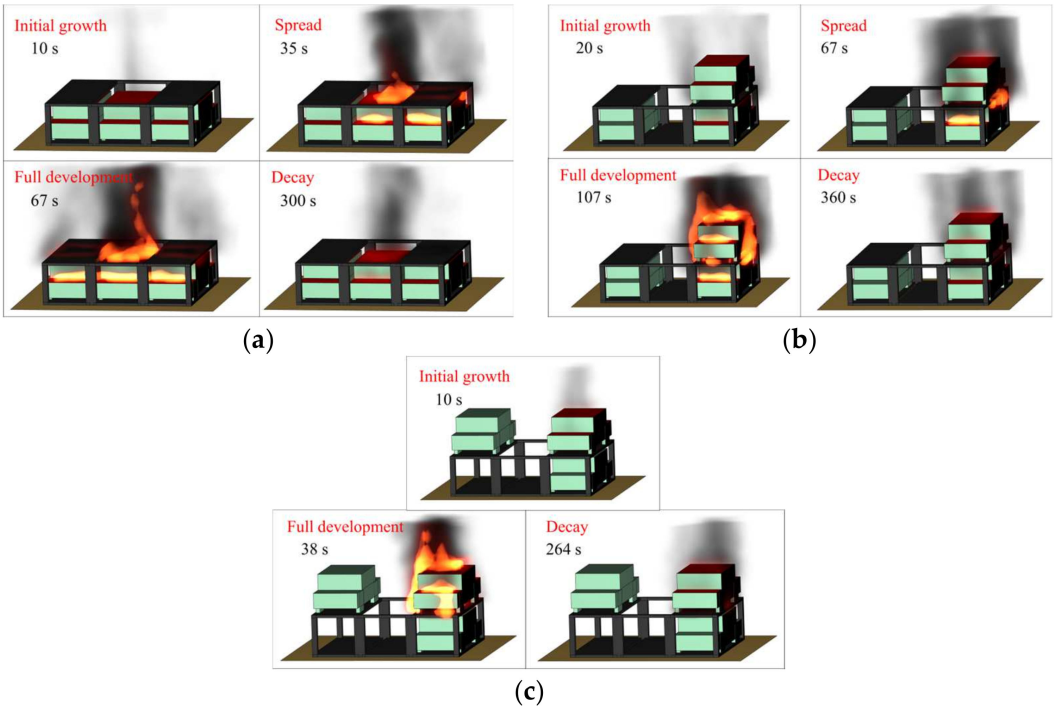

Figure 8. Simulation process of fires under different case conditions: (**a**) Case 1, (**b**) Case 2, and (**c**) Case 3.

3.2.2. Temperature Results of FDS

The temperature variation in the parking spaces should be given special attention. The temperature–history curves for the five parking spaces in each case are shown in Figure 9. Compared to the temperature variation curves from the experiment in Figure 5, the simulated temperature trends are generally consistent. This demonstrates that the fire characteristics of the outdoor mechanical car garage are effectively reflected in the reduced-scale experiments. In the simulation results, the temperature of the unburned parking spaces is generally lower than that observed in the experiments, which is due to the difference in scale. The simulation scale is five times larger than the experimental scale, resulting in an increased relative distance for radiant and conductive heat transfer. As a result, the temperature at the measurement points is less affected by thermal feedback. Therefore, the temperatures of P4 and P5 in Case 1, as well as those of P2 in Cases 2 and 3, are lower than the experimental temperature. For the burning parking spaces, the average temperature during the full development with the open-top wall is higher than that with the limited-top wall.

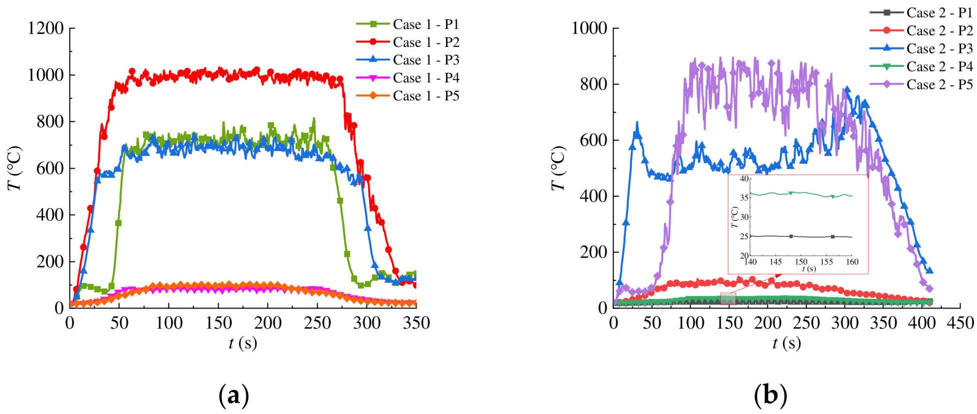

Figure 9. *Cont.*

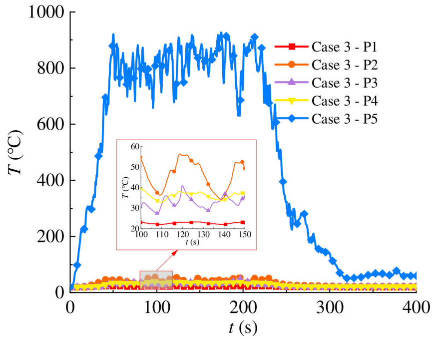

(**c**)

Figure 9. Simulation temperature results under different case conditions: (**a**) Case 1, (**b**) Case 2, and (**c**) Case 3.

To provide a clearer understanding of the temperature distribution during the full development of the fire, temperature contour slices are generated at the center of the front view and at a height of 1.75 m from the vertical view of the parking space, respectively. Particularly, the temperature distribution of the top wall in the parking space frame is visually observed through the temperature slice of the vertical view. The temperature distribution nephogram at around 160 s under different case conditions is presented in Figure 10. In condition 1 of Figure 10a, the flame temperature in parking space P2 is the highest, while the flame temperature in parking spaces P1 and P3 is relatively lower due to their locations in the narrow spaces between the car and the top wall. Unlike the flames in parking space P2 burning vertically upwards from the vent, the flames in parking spaces P1 and P3 collide with the top wall and spread around, leading to a larger flame-affected area compared to P2. Similarly, Figure 10b shows that the phenomenon of impacting surfaces and expanding high-temperature areas is more pronounced. In Figure 10c, the top wall temperature of the mechanical parking is slightly lower in Case 3 compared to the other case, which is caused by less heat being transferred downward from the fire of the P5 parking space.

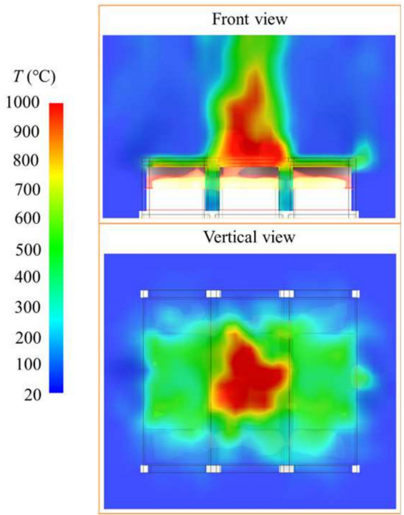

(**a**)

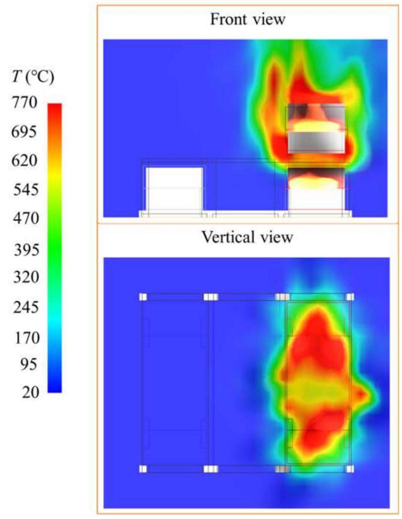

(**b**)

Figure 10. *Cont.*

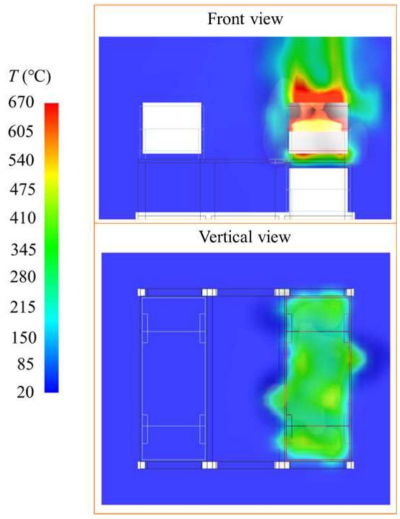

(**c**)

Figure 10. Temperature nephograms of mechanical parking space at around 160 s: (**a**) Case 1, (**b**) Case 2, and (**c**) Case 3.

3.2.3. Comparative Analysis of Simulation and Experiment

Using the simulation results of the temperature at parking space P1 in Case 1 as an illustrative example, a comparative analysis was conducted with the corresponding experimental data, as depicted in Figure 11. The simulation results showed good consistency with the experimental data, primarily due to the utilization of well-validated FDS simulations. Moreover, the trends in the rising and stable stages of the experimental and simulation results are consistent with the trends of the European standard (DIN EN 1993-1-2) [43]. Meticulous matching of simulation parameters to experimental conditions also contributed to the consistency. In addition, rigorous post-processing was conducted to extract comparable information. However, minor discrepancies existed, possibly stemming from model simplifications, experimental errors, scale differences, and measurement stability issues. To alleviate these differences, the simulation model can be optimized through stricter precision parameter settings. Overall, despite minor numerical deviations, the simulation effectively captured the experimental trends and behaviors.

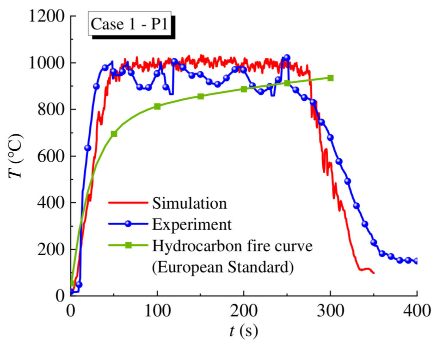

Figure 11. Comparison between experimental and simulation data of P1 in Case 1.

4. Finite Element Simulation

4.1. Finite Element Modeling

To obtain the high-temperature mechanical behavior of the parking spaces, the experimental fire temperature data are taken as input conditions using the sequential thermal coupling method. To save computational resources and quickly obtain the deformation characteristics of the mechanical parking spaces under fire conditions, a finite element model is established based on the full-scale dimensions of the front view. The model is divided into a grid with a cell size of 5 mm, resulting in a total of 82,200 elements. The thermal analysis is performed using a four-node convective/diffusive quadrilateral element (DCC2D4), and the mechanical analysis is conducted using a four-node, bilinear, reduced-integration, hourglass control plane stress element (CPS4R). The bottom is fully constrained. The thermal properties of materials are variable with temperature rising, but the thermal physical parameters of steel are generally considered constant for structural fire resistance calculation. Therefore, the specific heat is assumed to be 600 J·kg^{-1}·°C^{-1}. The thermal conductivity is 45 W·m^{-1}·°C^{-1}. The density is 7850 kg·m^{-3}, and the coefficient of thermal expansion is 1.4×10^{-5} °C^{-1}.

Q235 steel is selected as the steel material for the mechanical parking spaces, with a yield stress of 235 MPa. The design strength value of the structural steel at high temperatures is calculated using Equations (4)–(7) [44]. The elastic modulus and yield strength of the steel decrease with temperature, and the reduction factors are shown in Table 2.

$$f_{\mathrm{T}} = \eta_{\mathrm{sT}} f \tag{4}$$

$$\eta_{\mathrm{sT}} = \begin{cases} 1.0 & 20\ ^\circ\mathrm{C} \le T_{\mathrm{s}} \le 300\ ^\circ\mathrm{C} \\ 1.24 \times 10^{-8} T_s^3 – 2.096 \times 10^{-5} T_s^2 & \\ +9.228 \times 10^{-3} T_s – 0.2168 & 300\ ^\circ\mathrm{C} < T_{\mathrm{s}} < 800\ ^\circ\mathrm{C} \\ 0.5 – T_s/2000 & 800\ ^\circ\mathrm{C} \le T_s \le 1000\ ^\circ\mathrm{C} \end{cases} \tag{5}$$

where T_{s} represents the temperature of the steel; f_{T} represents the design strength of the steel at high temperatures; f represents the design strength of the steel at room temperature; and η_{sT} is the reduction factor for the yield strength of the steel at high temperatures.

$$E_{\mathrm{sT}} = \chi_{\mathrm{sT}} E_s \tag{6}$$

$$\chi_{\mathrm{sT}} = \begin{cases} \frac{7T_s - 4780}{6T_s - 4760} & 20\ ^\circ\mathrm{C} \le T_s < 800\ ^\circ\mathrm{C} \\ \frac{1000 - T_s}{6T_s - 2800} & 800\ ^\circ\mathrm{C} \le T_s \le 1000\ ^\circ\mathrm{C} \end{cases} \tag{7}$$

where E_{sT} represents the elastic modulus of the steel at high temperatures; E_{s} represents the elastic modulus of the steel at room temperature; and χ_{sT} is the reduction factor for the elastic modulus of the steel at high temperatures.

Table 2. Reduction factors for high temperatures of steel.

***T* (°C)**	**20**	**100**	**200**	**300**	**400**	**450**	**500**	**550**	**600**	**650**	**700**	**750**	**800**	**900**	**1000**
χ_{sT}	1	0.98	0.95	0.91	0.84	0.79	0.73	0.64	0.50	0.32	0.21	0.15	0.10	0.04	0
η_{sT}	1	1.00	1.00	1.00	0.91	0.82	0.71	0.58	0.45	0.33	0.23	0.15	0.10	0.05	0

4.2. Stress Analysis

In the model of the mechanical parking space, the top wall and columns are components directly exposed to the high-temperature field of the fire, which are more prone to structural damage. Therefore, the time–history curves of the average Mises stresses in the top wall and columns of parking spaces P1, P2, and P3 under each case condition are plotted in Figure 12.

In Case 1, the column of parking space P2 fails at 10 s, followed by the failure of the top plate and column of parking space P3 at 12 s. This indicates that the limit stress values of elasticity and yield are exceeded by the rapid heating and propagation of parking spaces P2 and P3, resulting in the inability of the top wall and columns to bear thermal loads. The stress growth of parking space P1 lags behind that of parking spaces P1 and P2. The stress value of 235 MPa in the column of parking space P1 is reached at 115 s, and the yield state is subsequently maintained. At 168 s, the structure is destroyed. The stress in the top plate of P1 shows an increasing trend followed by a decreasing trend. The peak stress occurs at 49 s with a value of 180 MPa.

In Case 2, the yield state of the column in parking space P3 is first reached at 33 s. After 44 s of maintenance, the stress rapidly decreases until it disappears. A peak stress of 67 MPa in the top wall of parking space P3 is experienced at 168 s. Then, the stress gradually decreases until it reaches zero. The stress in the column of parking space P2 increases continuously with time and reaches 205 MPa at 184 s. The column of parking space P1 rapidly increases to 89 MPa at the initial moment, and then the stress continues to increase. At 167 s, the column of parking space P1 began to yield and failed for 13 s. The top wall stress of the P1 parking space is always low. The calculated value at the final moment is only 18 MPa. After structural failure, the stress rapidly decreases to 0 MPa.

In Case 3, the entire duration is set to 600 s, covering the entire process of the fire. Since parking space P5 is on fire, it has the greatest impact on the column of parking space P2, with the stress continuously increasing. A high-stress value of 206 MPa at the final time is reached. The columns of parking spaces P1 and P3 show a trend of increasing and then decreasing, with an obvious turning point at 394 s. The top wall of P3 rapidly increases to 85 MPa in the early stage of the fire, followed by slow growth. The maximum peak stress is 102 MPa at 202 s, and then the stress slowly decreases. The top wall of parking space P1 is minimally affected throughout the fire duration, reaching only 23 MPa at the final time.

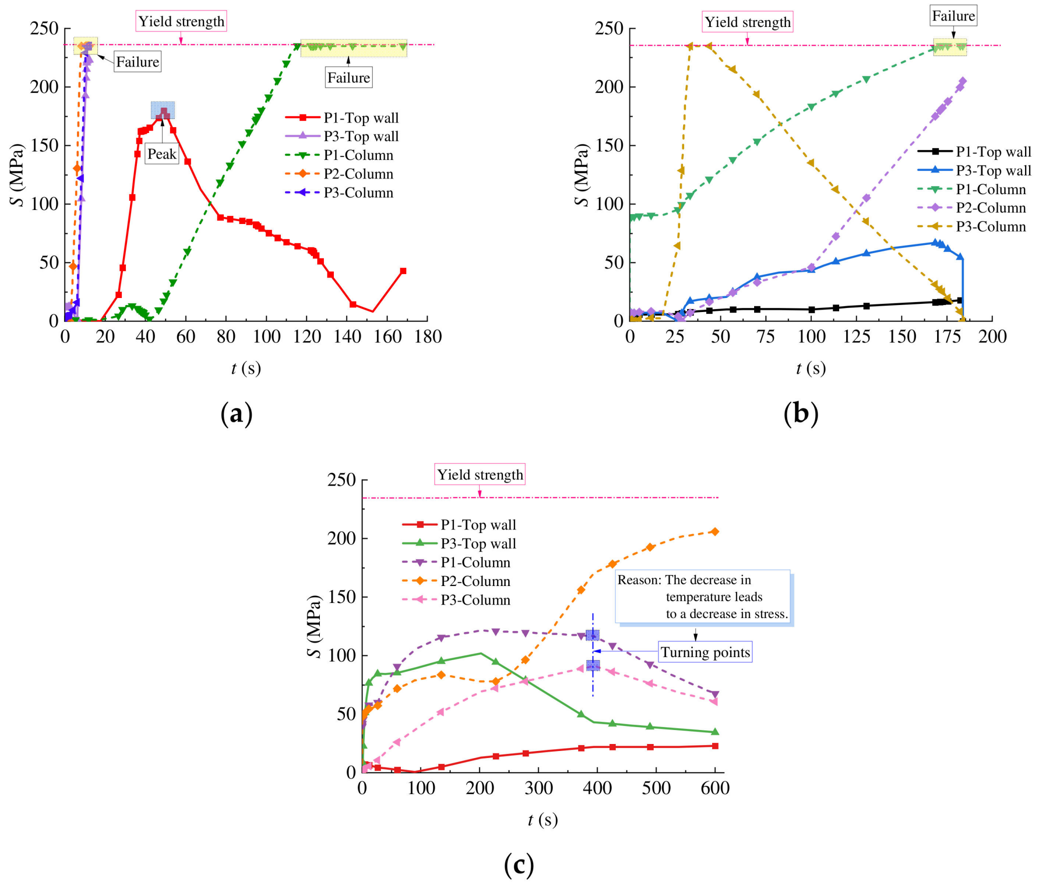

Figure 12. Time–history stress profiles of top walls and columns: (**a**) Case 1, (**b**) Case 2, and (**c**) Case 3.

The stress contour plots for the fire process in the mechanical parking spaces are depicted in Figure 13. Meanwhile, considering the temporal relationship profiles in Figure 12, it can be observed that parking spaces P1, P2, and P3 in Case 1 are all unsafe, and the structures fail in sequence as the fire spreads. In Case 2, although only parking space P3 is on fire, the column of parking space P1 eventually fails, indicating that both P1 and P3 are unsafe. In Case 3, no failure occurs, but parking space P2 is relatively more dangerous.

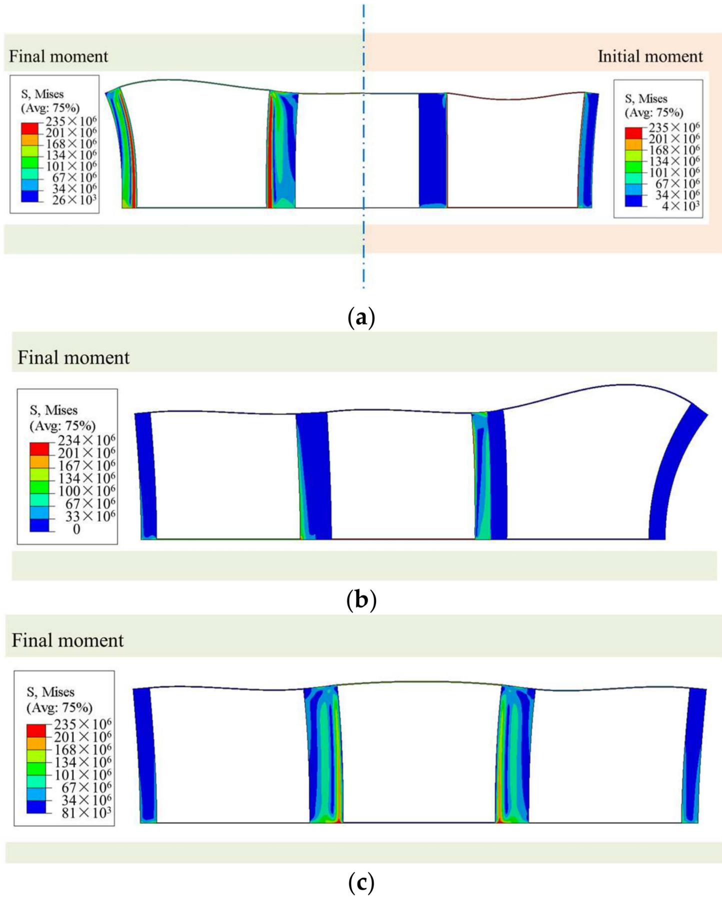

Figure 13. Stress contour plots: (**a**) Case 1, (**b**) Case 2, and (**c**) Case 3.

4.3. Displacement Analysis

Figure 14 shows the maximum deformations of the top walls and columns of parking spaces P1, P2, and P3 in all cases. The time–history curves of the deformations of the columns and top walls of the same parking space in the three cases exhibit consistent trends, indicating that the top walls and columns are co-deformed, with mutual promotion and driving effects.

In Figure 14a, when the top plates and columns of parking spaces P2 and P3 fail, their deformations are 4.1 mm, 3.4 mm, and 0.6 mm, respectively. This indicates that even small deformations under severe high-temperature fire are sufficient to cause damage and failure of the structure. The deformation of parking space P1 increases rapidly with increasing temperature, reaching its first peak at 49 s, with deformations of 8.4 mm and 6.1 mm for the top wall and column, respectively. Subsequently, there is a slight attenuation in the deformation amount, which stops at 67 s. Afterward, the deformation increases again and reaches the second peak at 122 s. At this moment, the deformations of the top wall and column in parking space P1 are 11.2 mm and 7.3 mm, respectively. After 122 s, the deformation begins to decrease. At the time of failure, the deformations of the top wall and column in parking space P1 are 10.3 mm and 6.7 mm, respectively. The reason for this deformation trend in the P1 parking space is that the deformation of the P1 parking space before 49 s is dominated by top plate stress. After 49 s, the top wall stress decreases while the column stress increases, intersecting at 67 s. After 67 s, the deformation of parking space P1 is dominated by the stress in the column.

Figure 14b indicates that the P3 parking space at the location of the fire has the most severe deformation. As time passes, the deformations of the top wall and column of parking space P3 continuously increase, with similar values. The top wall and column deformation at the final failure time is approximately 21 mm. Parking space P1 experiences minor deformations, with a final deformation of approximately 3 mm. However, the P2 parking space only undergoes a deformation of 1.2 mm in the end.

All parking spaces in Figure 14c experienced certain deformations to varying degrees, showing a trend of initial increase followed by decrease. Parking space P3, located adjacent to the fire origin at P5, is the most affected. The deformation of the top wall and column in parking space P3 rapidly increased to 6.9 mm and 8.6 mm, respectively, within the first 26 s. From 26 s to 202 s, the deformation of P3 continued to increase slowly and reached its peak at 202 s. The peak deformations of the top wall and column of P3 were 9.4 mm and 10.8 mm, respectively. From 202 s to 394 s, the deformation of P3 quickly dropped to around 5 mm. From 394 s to 600 s, the deformation of P3 decreased slowly. In the final moment, the deformations of the top slab and column of P3 were 4 mm and 3.7 mm, respectively. The deformations of P1 and P2 were minimal with similar deformation trends. From 202 s to 394 s, the deformations of the top wall and column of P1 and P2 reached their maximum values and remained stable at 4.4 mm, 4.9 mm, and 2.9 mm, respectively.

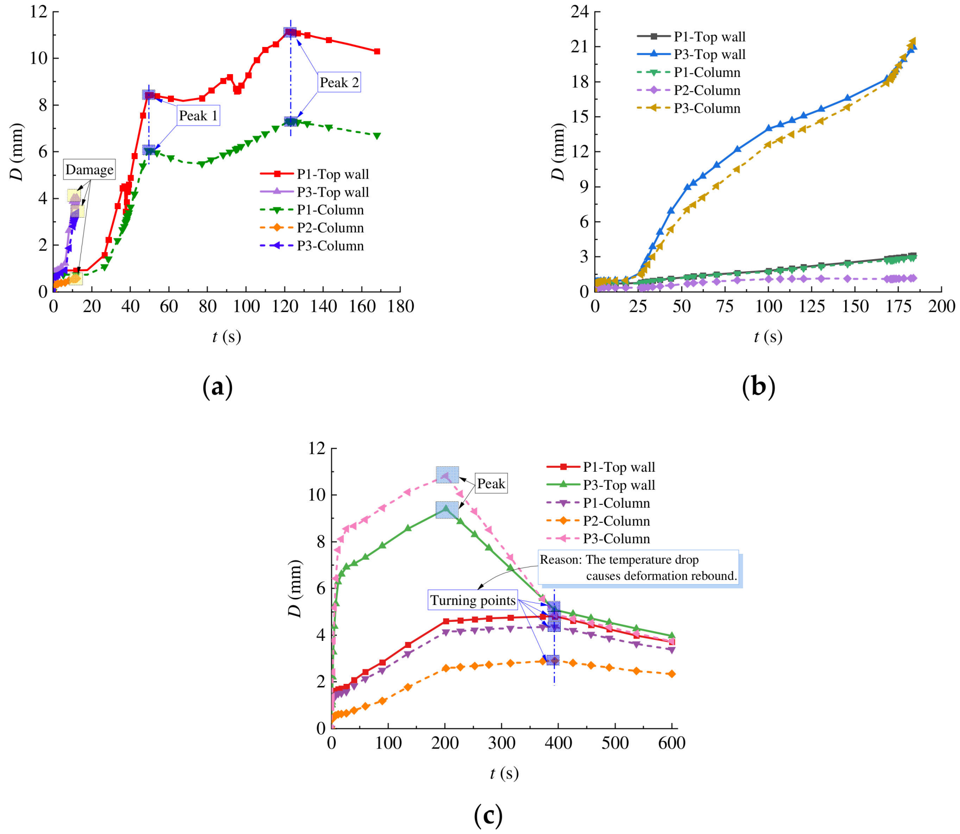

Figure 14. Time–history deformation profiles of top walls and columns: (**a**) Case 1, (**b**) Case 2, and (**c**) Case 3.

5. Fire Protection Design

To protect mechanical three-dimensional parking spaces and reduce the temperature of the ceiling and columns during a fire, a fire protection method is designed and proposed in this article. Composed of a multi-layer structure, the fire protection design features inner and outer support layers sandwiched with perlite material. A steel cylinder section with a diameter of 100 mm was simulated to determine its temperature field distribution, as depicted in Figure 15a. Using the same high-temperature load as the unprotected calculation, the temperature field of the protected circular rod section was calculated. The thickness of the protective layer was 10 mm. The results are shown in Figure 15b. It was found that the central temperature decreased from 950.34 °C to 270.49 °C, a reduction of 71.5%, indicating good protective effects.

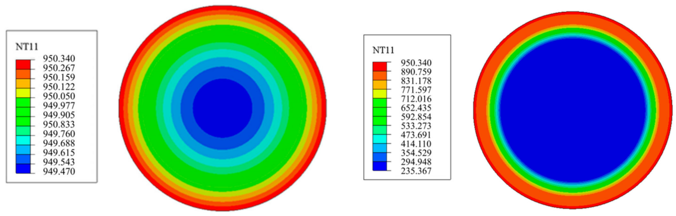

(**a**) (**b**)

Figure 15. Temperature field under fire: (**a**) unprotected structure; (**b**) with protective structure.

This protective method was applied to Cases 1, 2, and 3, respectively, with a protective thickness of 10 mm. Measurement points were placed at the center of each parking space ceiling plane and the middle height of each column, and the temperature results were obtained as shown in Figure 16. As shown in Figure 16a, the peak loading temperature reached 854 °C, yet the corresponding temperatures for the top wall and column of P1 were recorded at 24 °C and 18 °C, respectively, indicating a remarkable temperature reduction of approximately 98%. Similarly, in Figure 16b, with a maximum loading temperature of 774 °C, the top wall and column of P3 maintained temperatures of 22 °C and 19 °C, respectively, demonstrating a temperature drop of nearly 97%. Furthermore, in Figure 16c, despite a peak loading temperature of 438 °C, the column of P2 maintained a temperature of 18 °C, reflecting a temperature reduction of approximately 96%. Evidently, the 10 mm thick fire protection device introduced in this article exhibits exceptional cooling efficiency and proven safety and effectiveness.

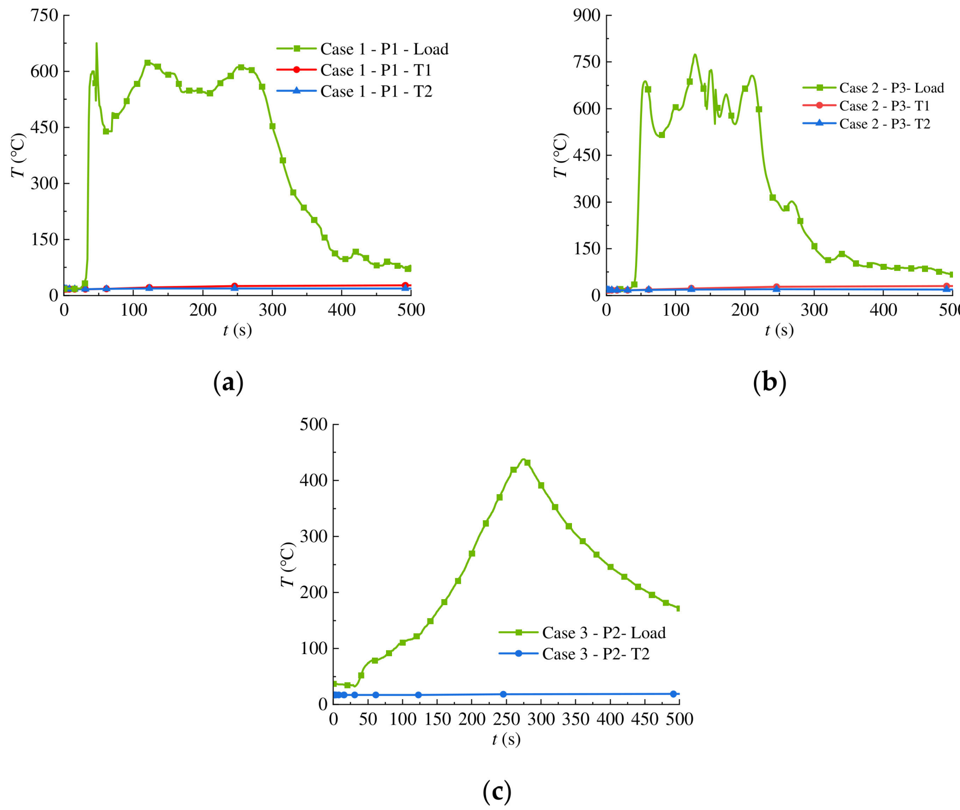

Figure 16. Fire prevention effects under different working conditions: (**a**) Case 1, (**b**) Case 2, and (**c**) Case 3.

6. Conclusions and Prospects

6.1. Conclusions

Based on the results of the comprehensive small-scale garage experiments, full-scale FDS simulations, and finite element analysis, the following conclusions can be drawn:

1. The experiments demonstrate that fire spread can be effectively blocked through interval parking spaces, while adjacent spaces are vulnerable to fire propagation. During the fire process, temperature data exhibit a highly consistent trend with fire behavior, encompassing the initial growth, full development, and decay stages.
2. When simulating with FDS, the reduced-scale model is restored to full size for testing. The simulation results align closely with the combustion process observed in the scale test. Through FDS temperature nephogram slices, the temperature distribution throughout the fire is observed more clearly. The diffusion of the flame upon hitting the top wall expands the high-temperature area on the wall.
3. Finite element simulations reveal that in Case 1, parking spaces P1, P2, and P3 are all unsafe and fail consecutively during the fire. In Case 2, the ultimate failure of the column in parking space P1 results from the fire in P3. In Case 3, P2 is relatively more hazardous, with stress reaching 206 MPa at 600 s. Additionally, deformation analysis shows a consistent trend in the deformation of the top wall and columns, indicating their coordinated deformation behavior. Under significant high-temperature exposure from the fire, even minor deformations can trigger structural failure.

In summary, the results from the experiments, FDS, and finite element analysis collectively demonstrate that the ignition source location, parking layout, and top wall structure have a significant influence on the development and propagation of fires in mechanical parking garages. Therefore, in the design and planning of mechanical parking garages, it is necessary to fully consider fire safety. Meanwhile, appropriate fire prevention measures should be implemented to mitigate potential risks, ensuring the safety and sustainability of parking areas. These conclusions provide a strong basis for the fire safety of mechanical parking garages and underscore the critical safety considerations necessary in parking design and management.

6.2. Prospects

With the increasing popularity and application of new energy vehicles, their fire safety issues are becoming increasingly prominent. Therefore, in future research work, the related issue of the impact of electric vehicle fires on the structure of mechanical parking lots will be prioritized for exploration, with the aim of comprehensively and thoroughly studying prevention and response strategies for car fires.

Author Contributions: Conceptualization, Y.L. and Z.W.; methodology, Y.Z. and Z.G.; validation, Y.L. and Y.Z.; formal analysis, Z.W. and H.M.; investigation, H.M. and Z.W.; resources, Z.W.; data curation, H.M.; writing—original draft preparation, Y.L. and Y.Z.; writing—review and editing, Y.L., Y.Z. and Z.G. All authors have read and agreed to the published version of the manuscript.

Funding: This research was funded by the National Natural Science Foundation of China under grant No. 52278301, Heilongjiang Provincial Key Laboratory of Nuclear Power System and Equipment Open-end Funds under grand No. HLJS202202, and Graduate Innovation and Entrepreneurship Practice Project of Anhui Province under grand No. 2022cxcysj028.

Institutional Review Board Statement: Not applicable.

Informed Consent Statement: Not applicable.

Data Availability Statement: The raw data supporting the conclusions of this article will be made available by the authors, without undue reservation.

Conflicts of Interest: The authors declare no conflicts of interest.

References

1. Mikusova, M.; Abdunazarov, J.; Zukowska, J.; Jagelcak, J. Designing of Parking Spaces on Parking Taking into Account the Parameters of Design Vehicles. *Computation* **2020**, *8*, 71. [CrossRef]
2. Wang, Z.; Zhu, G.; Zhou, J.; Chai, G.; Wang, P. Experimental Study on Fire Propagation and Temperature Distribution of Passenger Car under Different Opening Conditions. *Case Stud. Therm. Eng.* **2019**, *14*, 100472. [CrossRef]

3. Zhu, H.; Gao, Y.; Guo, H. Experimental Investigation of Burning Behavior of a Running Vehicle. *Case Stud. Therm. Eng.* **2020**, *22*, 100795. [CrossRef]
4. Terziev, A.; Antonov, S. Experimental Study on the Transfer of Fire from a Burning Car to a Neighboring One. In Proceedings of the 2019 International Conference on ENERGY and ENVIRONMENT (CIEM), Timisoara, Romania, 17–18 October 2019; pp. 19–23.
5. Okamoto, K.; Ichikawa, T.; Shimizu, K.; Honma, M. Thermal Effect on Surrounding Combustibles in Minivan Passenger Car Fires. *Fire Mater.* **2018**, *42*, 583–592. [CrossRef]
6. Brzezinska, D.; Ollesz, R.; Bryant, P. Design Car Fire Size Based on Fire Statistics and Experimental Data. *Fire Mater.* **2020**, *44*, 1099–1107. [CrossRef]
7. Truchot, B.; Fouillen, F.; Collet, S. An Experimental Evaluation of Toxic Gas Emissions from Vehicle Fires. *Fire Saf. J.* **2018**, *97*, 111–118. [CrossRef]
8. Dorsz, A.; Lewandowski, M. Analysis of Fire Hazards Associated with the Operation of Electric Vehicles in Enclosed Structures. *Energies* **2022**, *15*, 11. [CrossRef]
9. Li, D.; Zhu, G.; Zhu, H.; Yu, Z.; Gao, Y.; Jiang, X. Flame Spread and Smoke Temperature of Full-Scale Fire Test of Car Fire. *Case Stud. Therm. Eng.* **2017**, *10*, 315–324. [CrossRef]
10. Luo, J.; Zhang, X.; Zhao, J.; Xu, Z. Fire Experiment on Temperature Distribution in an Underground Vertical Car Park. *Case Stud. Therm. Eng.* **2019**, *15*, 100513. [CrossRef]
11. Barsim, M.M.; Bassily, M.A.; El-Batsh, H.M.; Rihan, Y.A.; Sherif, M.M. Performance of Impulse Ventilation System in an Underground Car Park Fire: Case Study. *J. Build. Eng.* **2020**, *29*, 101162. [CrossRef]
12. Špiljar, Ž.; Schneider, D.R.; Drakulić, M. Analysis of Smoke Stratification and Smoke Layer Thickness in Underground Car Parks. *Therm. Sci.* **2018**, *22*, 1963–1972. [CrossRef]
13. Hertz, K.D.; Sørensen, L.S.; Giuliani, L. Reliable Assumptions for Structural Fire Design of Steel Car Parks. *J. Struct. Fire Eng.* **2021**, *13*, 32–48. [CrossRef]
14. Boehmer, H.R.; Klassen, M.S.; Olenick, S.M. Fire Hazard Analysis of Modern Vehicles in Parking Facilities. *Fire Technol.* **2021**, *57*, 2097–2127. [CrossRef]
15. Yan, X.; Charlier, M.; Gernay, T. Thermal Response of Steel Framing Members in Open Car Park Fires. *Front. Struct. Civ. Eng.* **2022**, *16*, 1071–1088. [CrossRef]
16. Shin, J.; Lee, H.; Min, J.-K.; Choi, I.-R.; Choi, S.-M. Predicting Temperature Loads in Open Car Parks of Piloti Structures Exposed to Real Fire Accidents. *Int. J. Steel Struct.* **2022**, *22*, 1889–1907. [CrossRef]
17. Deckers, X.; Haga, S.; Tilley, N.; Merci, B. Smoke Control in Case of Fire in a Large Car Park: CFD Simulations of Full-Scale Configurations. *Fire Saf. J.* **2013**, *57*, 22–34. [CrossRef]
18. Bacak, A. Numerical Investigation of Impulse Ventilation System in Underground Car Park. *Int. J. Eng. Appl. Sci.* **2017**, *4*, 257525.
19. Deckers, X.; Haga, S.; Sette, B.; Merci, B. Smoke Control in Case of Fire in a Large Car Park: Full-Scale Experiments. *Fire Saf. J.* **2013**, *57*, 11–21. [CrossRef]
20. Merci, B.; Shipp, M. Smoke and Heat Control for Fires in Large Car Parks: Lessons Learnt from Research? *Fire Saf. J.* **2013**, *57*, 3–10. [CrossRef]
21. Selamet, S.; Ayva, B. Car Fires in Multi-Story Parking Garages. *Turk. J. Civ. Eng.* **2023**, *34*, 83–110. [CrossRef]
22. Koromila, I.A.; Spyrou, K.J. Design Fire Methodology for Vehicle Spaces Onboard Ships. *Fire Technol.* **2023**, *59*, 1725–1759. [CrossRef]
23. Gavryliuk, A.; Yakovchuk, R.; Ballo, Y.; Rudyk, Y. Thermal Modeling of the Electric Vehicle Fire Hazard Effects on Parking Building. *SAE Int. J. Trans. Saf.* **2023**, *11*, 421–434. [CrossRef]
24. Di Matteo, S. Fire Risk of Electric Vehicles in Confined Spaces. Master's Thesis, Politecnico di Torino, Turin, Italy, 2023.
25. Ma, R.; Cui, C.; Ma, M.; Chen, A. Numerical Simulation and Simplified Model of Vehicle-Induced Bridge Deck Fire in the Full-Open Environment Considering Wind Effect. *Struct. Infrastruct. Eng.* **2021**, *17*, 1698–1709. [CrossRef]
26. Ayva, B. Performance-Based Fire Safety Design for Automated Vehicle Parking Steel Structures. Master's Thesis, Bogazici University, Istanbul, Turkey, 2020.
27. Kumar, P.; Kodur, V. A Rational Approach for Fire-Resistance Evaluation of Double-Tee, Prestressed Concrete Slabs in Parking Structures. *PCI J.* **2020**, *65*, 20–41. [CrossRef]
28. Meng, F.; Mago, N.; Andisheh, K.; Clifton, G.C. Numerical Validation of Structural Fire Design for Steel Framed Car Park Buildings. *Fire Saf. J.* **2023**, *139*, 103819. [CrossRef]
29. Yang, Y.; Yang, W.; Zhang, Z.; Liu, F.; Frank Chen, Y. Fire-Resistant Test and Fire Protection Layer Research of U-Shaped Steel–Concrete Composite Beams. *Structures* **2023**, *58*, 105340. [CrossRef]
30. Bradford, M.A.; Liu, X.; Chen, C.; Wang, J. Finite Element Modelling of Lattice Angle Steel Structures Exposed to Wildland Fires. *Structures* **2023**, *56*, 104901. [CrossRef]
31. *JGJ 100-2015*; Code for Design of Parking Garage Building, Urban-Rural Development. Ministry of Public Security: Beijing, China, 2015.
32. *GB50067-97*; Code for Fire Protection Design of Garage, Motor Repair Shop and Parking Area. Ministry of Public Security: Beijing, China, 2014.

33. Lecocq, A.; Bertana, M.; Truchot, B.; Marlair, G. Comparison of the Fire Consequences of an Electric Vehicle and an Internal Combustion Engine Vehicle. In Proceedings of the International Conference on Fires in Vehicles—FIVE 2012, Chicago, IL, USA, 27–28 September 2012.
34. Krol, M.; Krol, A. The Threats Related to Parking Electric Vehicle in Underground Car Parks. In *Intelligent Solutions for Cities and Mobility of the Future, Proceedings of the 17th Scientific and Technical Conference "Transport Systems Theory and Practice 2021", Katowice, Poland, 21–23 September 2021*; Springer: Cham, Switzerland, 2022; pp. 72–81.
35. Brzezinska, D.; Bryant, P. Performance-Based Analysis in Evaluation of Safety in Car Parks under Electric Vehicle Fire Conditions. *Energies* **2022**, *15*, 649. [CrossRef]
36. Bai, J.; Liao, H.; Xia, Y. Study on Fire Accidents in Tunnels. *IOP Conf. Ser. Mater. Sci. Eng.* **2020**, *741*, 012095. [CrossRef]
37. Zhang, Q. Spontaneous Combustion of Lithium Batteries and Its Preventive Measures. *IOP Conf. Ser. Earth Environ. Sci.* **2021**, *677*, 052030. [CrossRef]
38. Fang, H.; Lo, S.M.; Zhang, Y.; Shen, Y. Development of a Machine-Learning Approach for Identifying the Stages of Fire Development in Residential Room Fires. *Fire Saf. J.* **2021**, *126*, 103469. [CrossRef]
39. Li, Z.; Zhang, S.; Cao, F. Analysis of Performance and Stability Factors of Vehicle Ethanol Gasoline for Motor Vehicle. *IOP Conf. Ser. Earth Environ. Sci.* **2020**, *514*, 042025. [CrossRef]
40. Santangelo, P.E.; Tarozzi, L.; Tartarini, P. Full-Scale Experiments of Fire Control and Suppression in Enclosed Car Parks: A Comparison between Sprinkler and Water-Mist Systems. *Fire Technol.* **2016**, *52*, 1369–1407. [CrossRef]
41. Kim, H.-J.; Lilley, D.G. Heat Release Rates of Burning Items in Fires. *J. Propuls. Power* **2012**, *18*, 866. [CrossRef]
42. Heskestad, G.; Delichatsios, M.A. The Initial Convective Flow in Fire. *Symp. Int. Combust.* **1979**, *17*, 1113–1123. [CrossRef]
43. *EN 1993-1-2*; Eurocode 3: Design of Steel Structures—Part 1-2: General Rules - Structural Fire Design. European Union: Brussels, Belgium, 2005.
44. Cui, C.; Chen, A.; Ma, R. Stability Assessment of a Suspension Bridge Considering the Tanker Fire Nearby Steel-Pylon. *J. Constr. Steel Res.* **2020**, *172*, 106186. [CrossRef]

Disclaimer/Publisher's Note: The statements, opinions and data contained in all publications are solely those of the individual author(s) and contributor(s) and not of MDPI and/or the editor(s). MDPI and/or the editor(s) disclaim responsibility for any injury to people or property resulting from any ideas, methods, instructions or products referred to in the content.